

---

This is an electronic reprint of the original article.  
This reprint may differ from the original in pagination and typographic detail.

Alkurdi, Susan S.A.; Al-Juboori, Raed; Bundschuh, Jochen; Bowtell, Les; Marcuk, Alla  
**Inorganic arsenic species removal from water using bone char**

*Published in:*  
Journal of Hazardous Materials

*DOI:*  
[10.1016/j.jhazmat.2020.124112](https://doi.org/10.1016/j.jhazmat.2020.124112)

Published: 05/03/2021

*Document Version*  
Peer-reviewed accepted author manuscript, also known as Final accepted manuscript or Post-print

*Published under the following license:*  
CC BY-NC-ND

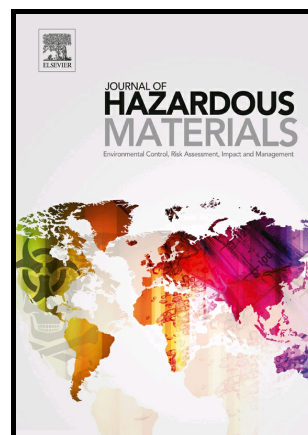
*Please cite the original version:*  
Alkurdi, S. S. A., Al-Juboori, R., Bundschuh, J., Bowtell, L., & Marcuk, A. (2021). Inorganic arsenic species removal from water using bone char: A detailed study on adsorption kinetic and isotherm models using error functions analysis. *Journal of Hazardous Materials*, 405, Article 124112.  
<https://doi.org/10.1016/j.jhazmat.2020.124112>

---

This material is protected by copyright and other intellectual property rights, and duplication or sale of all or part of any of the repository collections is not permitted, except that material may be duplicated by you for your research use or educational purposes in electronic or print form. You must obtain permission for any other use. Electronic or print copies may not be offered, whether for sale or otherwise to anyone who is not an authorised user.

Inorganic arsenic species removal from water using bone char: A detailed study on adsorption kinetic and isotherm models using error functions analysis

Susan S.A. Alkurdi, Raed A. Al-Juboori, Jochen Bundschuh, Les Bowtell, Alla Marchuk



PII: S0304-3894(20)32102-6

DOI: <https://doi.org/10.1016/j.jhazmat.2020.124112>

Reference: HAZMAT124112

To appear in: *Journal of Hazardous Materials*

Received date: 11 July 2020

Revised date: 19 September 2020

Accepted date: 24 September 2020

Please cite this article as: Susan S.A. Alkurdi, Raed A. Al-Juboori, Jochen Bundschuh, Les Bowtell and Alla Marchuk, Inorganic arsenic species removal from water using bone char: A detailed study on adsorption kinetic and isotherm models using error functions analysis, *Journal of Hazardous Materials*, (2020) doi:<https://doi.org/10.1016/j.jhazmat.2020.124112>

This is a PDF file of an article that has undergone enhancements after acceptance, such as the addition of a cover page and metadata, and formatting for readability, but it is not yet the definitive version of record. This version will undergo additional copyediting, typesetting and review before it is published in its final form, but we are providing this version to give early visibility of the article. Please note that, during the production process, errors may be discovered which could affect the content, and all legal disclaimers that apply to the journal pertain.

© 2020 Published by Elsevier.

**Inorganic arsenic species removal from water using bone char: A detailed study on adsorption kinetic and isotherm models using error functions analysis**

Susan S.A. Alkurdi<sup>a,b</sup>, Raed A. Al-Juboori<sup>c</sup>, Jochen Bundschuh<sup>a,d\*</sup>, Les Bowtell<sup>e</sup>, Alla Marchuk<sup>f</sup>

<sup>a</sup> *School of Civil Engineering and Surveying, Faculty of Health, Engineering and Sciences, University of Southern Queensland, West Street, Toowoomba, 4350, Queensland, Australia.*

<sup>b</sup> *Northern Technical University, Engineering Technical College/Kirkuk, Iraq.*

<sup>c</sup> *Water Engineering Research Group, Department of Civil and Environmental Engineering, Aalto University, P.O. Box 15200, Aalto, FI-00076 Espoo, Finland.*

<sup>d</sup> *UNESCO Chair on Groundwater Arsenic within the 2030 Agenda for Sustainable Development, University of Southern Queensland, West Street, Toowoomba, 4350, Queensland, Australia.*

<sup>e</sup> *School of Mechanical and Electrical Engineering, Faculty of Health, Engineering and Sciences, University of Southern Queensland, Toowoomba, 4350, QLD, Australia.*

<sup>f</sup> *University of Southern Queensland, Centre for Sustainable Agricultural Systems, Toowoomba, 4350, Queensland, Australia.*

Corresponding author\*: Jochen Bundschuh

Faculty of Health, Engineering and Sciences & UNESCO Chair on Groundwater Arsenic within the 2030 Agenda for Sustainable Development, University of Southern Queensland, West Street, Toowoomba, 4350, Queensland, Australia.

Phone: +61 7 4631 2694

Email: Jochen.Bundschuh@usq.edu.au

## Abstract

The removal of inorganic arsenic (As) species from water using bone char pyrolyzed at 900 °C was investigated. Results revealed that the Sips model resulted in the best As(III) experimental data fit, while As(V) data was best represented by the Langmuir model. The adsorption rate and mechanisms of both As species were investigated using kinetic and diffusional models, respectively. At low As(III) and As(V) concentrations of 0.5 and 2.5 mg/L, the removal was due to intra-particle interactions and pore diffusion following Pseudo-first-order kinetics. However, at higher concentrations of 5 and 10 mg/L, the pore diffusion mechanism was ineffective, and the adsorption was best described by Pseudo-second-order and Elovich models. The goodness of the fit of linearized and nonlinear forms of all models against experimental data was tested using thorough error function analysis. Nonlinear regressions produced lower error values, so they were utilized to calculate the parameters of the models. The changes in bone char surface chemistry were examined using FTIR and Energy-dispersive X-ray spectroscopy (EDS). Arsenic oxide and complexes with metals were the confirmed immobilized forms of As on the bone-char surface. To the authors' knowledge, this study is the first attempt at As(III) adsorption analysis using bone char.

## Keywords

Arsenic; kinetic models; isotherm models; bone char.

## 1. Introduction

Arsenic is found in groundwater originating from natural and anthropogenic sources constituting a global problem. Arsenic is classified as a Class I carcinogenic contaminant, and has affected millions of people globally causing chronic disease and death (Kumarathilaka et al., 2020). Arsenic in groundwater is derived from the weathering and erosion of the crystalline and sedimental rocks (Yadav et al., 2020). Many countries, especially in Asia, the Americas and Europe source potable water from groundwater with As concentration much higher than the recommended limit for drinking water of 10 µg/L (WHO, 2011). Inorganic As is the dominant form of As in groundwater represented by arsenite [As(III)] and arsenate

[As(V)]. Under reducing conditions, As(III) which is the most toxic and mobile phase of As is the dominant inorganic As species in groundwater (Amen et al., 2020; Shaheen et al., 2019). For instance, Kumar and Ramanathan (2019) reported that 74% of samples from different areas in Central India, West Bengal and Bangladesh, where reducing aquifers dominate, show a prevalence of As(III) in their groundwater. The significant population size and low socio-economic status of these communities highlights the need for development of sustainable and low-cost As removal technologies.

Recently, a number of researchers investigated As(V) and As(III) removal from water using different adsorbent materials and methods (Liu et al., 2020), such as activated carbon (Dieme et al., 2017; Hashim et al., 2019; Kalaruban et al., 2019), zeolite (Meher et al., 2016; Soni and Shukla, 2019), biochar (Niazi et al., 2018b; Singh and Mohan, 2020; Tabassum et al., 2019). Waste-based adsorbents from the meat industry, such as bone char, can be a potential solution for the contamination problem. Bone char has been reported to be an excellent adsorbent for fluoride ions (F<sup>-</sup>) removal from water and discoloration in the sugar industry (Minja, 2020; Nigri et al., 2019). However, there are limited studies examined the use of bone char for As(V) removal (Alkurdi et al., 2019b) and not known studies for the removal of As(III) due to its less amenability to adsorption at natural pH range of groundwater where As(III) species are neutral (Zeltner, 2002). With regards to As(V), despite the availability of limited investigations that explored its removal with bone char, the mechanism of the removal is still not elucidated properly. The thermal transformation of the meat bones into bone char to be used for As removal recently has gained special interest in the field of water treatment (Alkurdi et al., 2020; Alkurdi et al., 2019a; Alkurdi et al., 2019b; Amin, 2020). Hence, this study is dedicated to scrutinizing As species adsorption onto bone char for the first time through detailed and careful examination for the effect of the treatment conditions on the efficiency and the nature of adsorption process.

The aim of this study was to investigate the adsorption of inorganic As species onto bone char under different treatment parameters such as pH, adsorbent concentration, adsorbate concentration and reaction time. Specific isotherms, kinetics and diffusion models were tested to gain a better understanding of the removal rate and behavior for different As species onto bone char. Error function analysis was applied to identify the mathematical models with the best fit for the obtained experimental data. EDS and FTIR were also applied to explore the changes in the bone char structure post adsorption and provide a better understanding of the removal mechanism.

## **2. Materials and methods**

### **2.1 Reagents and equipment**

All reagents were AR grade chemicals. Stock solutions of 1000 mg/L As(III) and As(V) in 2% HNO<sub>3</sub> were purchased from Choice Analytical, New South Wales, Australia. The pH of the test solutions was adjusted using 0.1 M nitric acid (70%, RCI Labscan) and sodium hydroxide (Labscan Asia Co. Ltd). The pH measurements were made using a TPS smart Chem-Lab pH meter. Arsenic assays were analyzed using ICP-MS (Perkin Elmer NEXION 300 ICP-MS). The adsorption of As species onto bone char surface was examined using EDS (JEOL JSM-7500FA). The applied accelerating voltage and probe current were 10 kV and 7.475 nA, respectively. The change in the structure of bone char particularly the alteration in functional groups was studied using FTIR (Amen et al., 2020).

### **2.2 Source and preparation of bone char**

The sheep bone waste was obtained from a local meat shop in Toowoomba, Australia. The bones were boiled and cut into small pieces and then pyrolyzed at 900 °C for 1 h, in a limited oxygen environment (Alkurdi et al., 2020). The pyrolysis conditions selected in this study

were based on the outcomes of our earlier investigations into the optimization of bone char for As removal (Alkurdi et al., 2020). This pyrolysis temperature provided the highest removal for both As(III) and As(V) when the removal efficiency was examined over a temperature range of 500 - 900 °C. The pyrolyzed bone char was washed with distilled water and then dried at 60 °C for 24 h, and then ground and sieved to the desired particle size (1 - 2 mm). The ground dried material was then sealed for later use in the adsorption experiments.

### 2.3 Sorption experiments

Batch sorption experiments were performed at room temperature ( $\approx 24$  °C). Each 50 ml test tube was filled with 15 mL of As(III) or As(V) solution of varying concentrations (1-50 mg/L) and adjusted to the optimum pH. The optimum pH for each As species was determined by examining the maximum As removal from water in the pH range 4-10 using 1 mg/L initial As concentration. A 5 g/L of bone char was added to each test tube and agitated for 4 h to reach equilibrium (based on the preliminary experiments). The optimal contact time and other conditions were selected on the basis of preliminary experiments which demonstrated that equilibrium was reached within 4 h. Then, the samples were filtered using Whatman No. 42 filter paper and analyzed for the final concentrations of As(III) and As(V) in the solution by ICP-MS. Arsenic concentrations retained in the adsorbent phase (mg/g) were calculated using the following formula:

$$q = \frac{C_0 - C_f}{W} * v \quad (1)$$

where  $q$  is the sorption capacity (mg/g),  $C_0$  and  $C_f$  are the initial and equilibrium concentrations (mg/L) of As in the solution,  $v$  is the volume (L) and  $W$  is the weight (g) of the adsorbent.

## 2.4 Isotherm models

To optimize the design of a sorption system, it is important to use adsorption isotherms to establish the appropriate correlation for the equilibrium curves. The experimental data of the As adsorption onto BC900 were substituted into equilibrium isotherm models to determine the best fit model for the removal process. Four different isotherm models were tested in this study. These models include two-parameters Langmuir and Freundlich models and three-parameters Redlich-Peterson (R-P) and Sips models.

The Langmuir isotherm model was originally proposed to describe gas adsorption onto activated carbon. Later, the Langmuir model was used to describe adsorption/desorption performance for different bio-sorbents. The Langmuir model is a chemical adsorption model that assumes a monolayer homogeneous adsorption process in which all sites provide an equal affinity to the adsorbate. The nonlinear form of the Langmuir model is given by:

$$q_e = \frac{Q_o k_L C_e}{1 + k_L C_e} \quad (2)$$

where  $k_L$  is Langmuir isotherm constant representing the ratio between the adsorption and desorption rate (L/mg),  $C_e$  is equilibrium concentration (mg/L),  $Q_o$  is the maximum coverage capacity estimated by the model (mg/g) and  $q_e$  is the amount of adsorbate at equilibrium (mg/g). Different linearized formulae were proposed for presenting equilibrium data. In this study, the formula presented below was used and compared to the non-linear regression results:

$$\frac{1}{q_e} = \frac{1}{Q_o} + \frac{1}{k_L Q_o C_e} \quad (3)$$

The Freundlich isotherm model represents an exponential distribution of the active sites of a heterogenous surface and its energy. It is an empirical equation that does not have a physical meaning (Wang and Guo, 2020). The nonlinear form of the Freundlich isotherm is given as:

$$q_e = K_F C_e^{1/n} \quad (4)$$

where  $K_F$  is the adsorption capacity ( $L^{1/n} \cdot mg^{1-1/n} \cdot g^{-1}$ ) and  $1/n$  is the adsorption intensity which represents the relative distribution of the heterogeneity and the energy of the adsorption sites. When the value of  $n = 1$ , the Freundlich model reduces to its linear form, while when  $n < 1$  or  $n > 1$  the adsorption process is described as favorable and unfavorable, respectively. These parameters may also be determined from the intercept and the slope of the linear trend after plotting the  $\log C_e$  versus  $\log q_e$  based on the linearized form of the model as shown in equation 5:

$$\log q_e = \log K_F + \frac{1}{n} \log C_e \quad (5)$$

The Redlich-Peterson (PR) model is a hybrid empirical formula incorporating three parameters from the amendment of the Langmuir and Freundlich isotherms, which assumes the presence of both homogeneous and heterogeneous surfaces on the adsorbent. The parameters of the nonlinear formula of this model (equation 6) were calculated by the nonlinear regression method:

$$q_e = \frac{K_{RP} C_e}{1 + a_{RP} C_e^{\beta_{RP}}} \quad (6)$$

where  $q_e$  is the experimental adsorption capacity (mg/g),  $C_e$  is the final concentration at equilibrium (mg/L),  $K_{RP}$  is the isotherm constant ( $L \cdot g^{-1}$ ),  $a_{RP}$  is the isotherm constant ( $L \cdot mg^{-1}$ ) and  $\beta_{RP}$  is the isotherm exponent. Based on the value of  $\beta_{RP}$ , the model either reduces to the Langmuir model at  $\beta_{RP} = 1$  or to linear model when  $\beta_{RP} = 0$  or  $C_e$  approaches 0 (Wang and Guo, 2020). On the other hand, if  $C_e$  approaches infinity, the model will reduce to Freundlich (Wang and Guo, 2020). The linearized form of this equation is:

$$\ln \left( k_{RP} \frac{C_e}{q_e} - 1 \right) = \beta_{RP} \ln C_e + \ln a_{RP} \quad (7)$$

Another three-parameters model that is a combination of the Langmuir and Freundlich models is the Sips model presented by the equation below:

$$q_e = \frac{a_m b C_e^{1/n}}{1 + b C_e^{1/n}} \quad (8)$$

while the linearized form of this model is:

$$\ln\left(\frac{q_e}{q_m - q_e}\right) = \frac{1}{n} \ln(c_e) + \ln(b)^{1/n} \quad (9)$$

where  $b$  is the Sips constant related to the energy of adsorption process and  $n$  is the exponential factor of the isotherm. At low adsorbate concentrations, the Sips model is reduced to the Freundlich equation. Then, the removal follows the Langmuir equation at higher concentrations (Kumara et al., 2014).

## 2.5 Kinetic models

Kinetic models provide an important tool to correctly evaluate the adsorption rate of contaminants. Four different kinetic models along with the intraparticle diffusion model were used to gain an understanding of the main removal behavior of As(III) and As(V). The Pseudo-first-order (PFO) model was tested by exercising the fitting procedure for the experimental removal of data against the theoretical model presented in Equation 10 (Qiu et al., 2009):

$$\ln\left(\frac{q_e - q}{q_e}\right) = -k_1 t \quad (10)$$

where  $q_e$  and  $q$  represent the amount of solute adsorbed at equilibrium and at any time of the adsorption (mg/g), respectively,  $k_1$  is the constant rate of first order sorption ( $\text{min}^{-1}$ ) and  $t$  is the time (s).

The Pseudo-second-order (PSO) rate equation assumes a second order uptake of the chemical constituents onto the surface of the adsorbent (Tan and Hameed, 2017). This model is expressed as:

$$q = \frac{q_e^2 k_2 t}{1 + q_e k_2 t} \quad (11)$$

where  $k_2$  is the Pseudo-second-order rate constant. These two models are widely applied to examine the removal of As from water on different adsorbents. For instance, Liu et al. (2014)

reported that the removal of As(V) from an aqueous solution followed the Pseudo-second-order model. Similarly, Darvishi Cheshmeh Soltani et al. (2017) reported that the removal of As(V) on Fe<sub>2</sub>O<sub>3</sub>/bone char nanocomposite followed the Pseudo-second-order model.

The Elovich model was established in 1937 by Zeldowitsch to identify the rate of chemisorption reaction (Qiu et al., 2009). This model does not account for desorption with an assumption that the equilibrium occurs over a long period of time (Tan and Hameed, 2017). The Elovich equation was first used to interpret the data of CO removal on manganese oxide (Tan and Hameed, 2017). The linearized form of this model is given by equation 12:

$$q = \frac{1}{\beta} \ln(\alpha\beta) + \frac{1}{\beta} \ln t \quad (12)$$

where  $\alpha$  is the initial adsorption rate in mg/g.min and  $\beta$  is the desorption constant. The plot of  $\ln t$  versus  $q$  should provide a straight line, for which the slope is  $1/\beta$  and the intercept represents  $\ln(\alpha\beta)/\beta$ . This model was found to fit the data of cadmium removal on bone char very well ( $R^2 > 0.99$ ) (Cheung et al., 2000). Similarly, Cheung et al. (2001) reported that the Elovich equation best fitted the removal of cadmium on bone char when compared to the Pseudo-first-order, Ritchie second order and Ritchie modified models.

The Ritchie equation was also used first for gas adsorption in 1977 (Ho, 2006). The model assumes that at  $t=0$ , the surface of the adsorbent is not occupied with any molecules and the adsorption rate is a function of the sites that are not occupied at time  $t$ . The rate of reaction using the Ritchie formula can be expressed as follows:

$$\frac{q_e}{q_e - q_t} = kt + 1 \quad (13)$$

where  $q_e$  is the amount of dye adsorbed at time  $t$  (mg/g),  $k$  is the rate constant of the Ritchie model ( $\text{min}^{-1}$ ) and  $t$  is the time (min).

### 2.5.1 Diffusional models

Understanding the dynamic behavior of an adsorption system is a pivotal step in the design and control of the treatment process. Adsorption processes take place throughout three stages, in which one or two of these stages are the controlling mechanisms of the removal. First, the adsorbent reaches the adjacent layers of the adsorbent particles. In next stage, the adsorbent particles diffuse through these adjacent layers to reach the pores on the surface. Finally, the interaction between the adsorbate and adsorbent takes place. The adsorption of targeted constituents in water onto adsorbents occurs through either intraparticle diffusion, pore diffusion, or the combination of these two mechanisms (Malash and El-Khaiary, 2010). Thus, the experimental data of As(III) and As(V) adsorption onto bone char was fitted to the aforementioned models to identify which model best describe the As species removal with bone char. In the case of the intra-particle diffusion model, the following formula was adopted in this study (Valderrama et al., 2008):

$$q_t = k_{ip}t^{0.5} + c \quad (14)$$

where  $q_t$  is the amount of adsorbed As (mg/g),  $k_{ip}$  is the rate constant of intraparticle diffusion model (mg/g min<sup>0.5</sup>) and  $c$  is the intercept. Fitting  $q_t$  versus  $t^{0.5}$  may provide a straight line indicating that the intraparticle diffusion is one of the controlling steps in the adsorption process (based on the value of  $c$ ). If the value of  $c$  is zero (the straight line passes through the origin), then the intraparticle is the main rate controlling step, otherwise there are other factors contributing to the process. If the plot is not a straight line, then different mechanisms are involved in the adsorption process other than intraparticle diffusion.

To test the contribution of the pore diffusion mechanism in As species removal on bone char, the Boyd model shown in equation 15 was applied (El-Khaiary and Malash, 2011). Following the same interpretation of the intraparticle model, the plot of  $B_t$  versus  $\ln(1 - q_t/q_e)$  from the Boyd model determines if the pore diffusion contributed to the adsorption process. This

kinetic model can be applied to differentiate between internal and external diffusion in the adsorption process (Ermolenko et al., 2020).

$$B_t = -0.4977 - \ln(1 - q_t/q_e) \quad (15)$$

where  $B_t$  is the mathematical function of the fractional attainment of equilibrium at different time ( $t$ ).

## 2.6 Data analysis

Analysis of variance (ANOVA) was carried out to test the differences between treatments. Five different error functions were used to compare the fit of the experimental data to the isotherm and kinetic models used to study As(III) and As(V) removal, based on the procedures described by Anirudhan and Radhakrishnan (2009) and Ho et al. (2002).

In brief, minimized errors were determined using the Solver add-in with Microsoft Excel software. Then, the sum of the normalized errors was calculated, by calculating the sum of the values achieved from the division of each error function by the function's maximum value for each run. These values were compared to each other and the minima were provided as the best fit of these models.

The standard error values which were used to ensure the accuracy of the data fitted to the models were the sum of the square of the error (SSE), hybrid fractional error function (HYBRID), Marquardt's percent standard deviation (MPSD), average relative error (ARE) and the sum of the absolute error (SAE). These standard errors were calculated applying the formulae (16-20) as presented below:

$$SSE = \sum_{i=1}^n (q_{exp} - q_{cal})_i^2 \quad (16)$$

$$HYBRID = \frac{100}{n-p} \sum_{i=1}^n \left[ \frac{(q_{exp} - q_{cal})^2}{q_{exp}} \right]_i \quad (17)$$

$$\text{MPSD} = \left[ \sqrt{\frac{1}{n-p} \sum_{i=1}^n \left( \frac{q_{exp} - q_{cal}}{q_{exp}} \right)_i^2} \right] * 100 \quad (18)$$

$$\text{ARE} = \frac{100}{n} \sum_{i=1}^n \left( \frac{|q_{exp} - q_{cal}|}{q_{exp}} \right)_i \quad (19)$$

$$\text{SAE} = \sum_{i=1}^n |q_{exp} - q_{cal}|_i \quad (20)$$

where  $q_{exp}$  is the experimental removal capacity (mg/g),  $q_{cal}$  is the theoretical removal capacity (mg/g),  $n$  is the number of data points and  $p$  is the number of the parameters for each model.

### 3. Results and discussion

#### 3.1 Summary of bone char characteristics

A detailed characterization of BC900 was presented in our previous study (Alkurdi et al., 2020). The effect of pyrolysis temperature on bone char ability to remove As(III) was not stated in the literature. However, a higher As(V) removal on bone char was observed at 500 °C compared to 900 °C (Czerniczyniec et al., 2007). Similarly, Begum et al. (2016) and Liu et al. (2014) reported the suitability of commercial bone char samples produced at 450 °C and 500 °C to remove As(V) from water. Table 1 shows the results for the BC900's characteristics.

#### 3.2 Sorption studies

##### 3.2.1 Effect of adsorbent dose

Adsorbent dose plays a significant role in the optimization of adsorption capacity. The effect of the adsorbent dose was examined by adding 2.5, 5 and 7.5 g/L of BC900 to 50 mL of 1 mg/L As(III) and As(V) aqueous solution and shaking for 4 h. It was observed that the

As(III) removal capacity increased from 0.009 mg/g to 0.079 mg/g with an increase in adsorbent dose from 2.5 to 5 g/L due to the increase in the availability of more adsorption sites occupying the adsorbate. However, further increase in BC900 dose to 7.5 g/L resulted in a decrease in As(III) uptake on the adsorbent to 0.009 mg/g.

A similar procedure for evaluating the effect of adsorbent dosage on As(V) adsorption was conducted. The removal capacity was increased from 0.075 mg/g to 0.11 mg/g after increasing the dose from 2.5 to 5 g/L, followed by a significant decrease to 0.03 mg/g after using 7.5 g/L BC900. Thus, the adsorbent dose for carrying out the rest of the experimental work was selected to be 5 g/L. Mondal and George (2015) studied the effect of adsorbent dose on the removal capacity of total As, As(III) and As(V) on activated carbon. The same trend with adsorbent levels was reported in their study as there was a positive relationship between the removal capacity and the adsorbent dose. However, after a certain limit of 8 g/L, there was no further increase in percentage removal (i.e. a decrease in removal when calculated on the basis of mg adsorbate per g adsorbent).

### 3.2.2 Effect of pH

To study the influence of solution pH on the adsorption of As(III) and As(V), experiments were performed with 1 mg/L initial concentration and 5 g/L adsorbent at different pH values. Since hydroxyapatite dissociates at low pH values <4 (Ramsey et al., 1973), therefore, the effect of pH was examined in the range of pH 4-12. Fig. 1 shows the changes in the removal capacity of BC900 at different pH values for As(III) and As(V). The removal capacity was increased as the initial pH was raised from 4 to 8.6 for As(III) and to 7.5 for As(V). Then, As uptake decreased after raising the pH value to 12. Similar observations were reported by Nicomel et al. (2016), where high pH favors As (III) removal and low pH promotes As(V) removal. The effect of pH on As(III) removal with bone char has not been addressed in previous studies. However, there has been a plethora of studies that investigated the optimum

pH values of As(V) removal using bone char. For example, Liu et al. (2014) and Begum et al. (2016) reported that the maximum As(V) removal on commercial bone char samples was achieved at pH 4. On the other hand, Chen et al. (2008) achieved the highest As(V) removal on a commercial bone char, but from a different source, at pH 10. The pH dependence of the adsorption process is mainly influenced by the overall charge of the adsorbent in an aqueous solution. As previously reported in Table 1, the point of zero charge ( $\text{pH}_{\text{pzc}}$ ) for BC900 is 8.3. The increases in As(V) uptake with increasing pH could be attributed to the electrostatic attraction of negatively charged As(V) species and the positively charged BC900 surface at pH values below  $\text{pH}_{\text{pzc}}$ . On the other hand, the maximum removal of As(III) was at a pH value greater than  $\text{pH}_{\text{pzc}}$ , which suggests that the mechanisms involved in the adsorption process of arsenite differ from those of arsenate. Zeta potential reached its highest value between pH 5 and 7. However, the higher removal capacity was not in the same range of high Zeta potential indicating the contribution of mechanisms other than electrostatic attraction in the removal. After identifying the optimum pH value for As species removal (i.e. pH of 8.6 for As(III) and 7.5 for As(V)), these pH values were applied in the kinetic and isotherm experiments.

### 3.2.3 Effect of initial As concentration

The effect of As concentration was studied with initial As(III) and As(V) concentrations ranging from 0.05 to 50 mg/L. Fig. 2. shows the adsorption capacity versus initial concentrations of As(III) (center line) and As(V) (dashed line), respectively. The figure shows that the adsorption capacity of As(III) increased with the initial concentration from 0.05 to 50 mg/L where the increased concentration provided the necessary driving force to oppose resistance toward the mass transfer of As(III) between the adsorbent and the adsorbate. However, the case is different for As(V) where the adsorption capacity increased

with an increase in the initial concentration up to 20 mg/L, and then decreased as the initial concentration increased to 50 mg/L. Comparing the effect of initial concentration to the results reported by Alam et al. (2018), but in a lower range of 0.5-5 mg/L, the same trend was noticed for both As species. Similar results were reported by Roy (2018) with a sharper decrease in the percentage removal of As(V) following the rise in the initial concentration to 0.5 mg/L using thioglycolated sugarcane carbon.

The maximum removal of As(III) was 2.543 mg/g at an initial concentration of 50 mg/L, while maximum removal of As(V) was achieved at the initial concentration of 20 mg/L with an equilibrium removal of 1.23 mg/g, and the removal capacity declined at 50 mg/L to 0.898 mg/g. The removal of As(III) was half the removal of As(V) at the same concentrations up to 2 mg/L. After this concentration, the uptake of As(III) reached almost the same value of As(V) removal at 20 mg/L before the removal trend reversed at 50 mg/L.

To design a fixed bed column for the purpose of continuous flow treatment, the contact time is of great importance in controlling removal efficiency. As can be seen from Fig. 2, As(V) had a higher removal rate when compared to As(III) removal at concentrations below 20 mg/L. With a maximum inorganic As concentration of <2 mg/L in natural groundwater globally (Herath et al., 2016; Mukherjee et al., 2006), bone char samples used in this study are more efficient in removing As(V) than As(III) at these concentrations ranges. However, with the higher percentage of As(III) in groundwater, due to its presence in reducing conditions, physical and chemical modification may be required to either improve the ability to remove As(III) or oxidize As(III) to As(V).

### 3.3 Sorption isotherm modeling

Fig. 3 shows the plot of the isotherm models and the experimental data for the As(III) and As(V) adsorption experiments in the range of 0.05-50 mg/L. It is clear from this figure that the experimental data of As(III) were well fitted with all of the isotherm models. However,

the comparison for the best fit were based on the coefficient of determination and minimal normalized errors provided in Tables 2 and 3.

Table 2 shows the values of the parameters calculated by nonlinear regression fits for the Langmuir and Freundlich isotherms along with the Redlich-Peterson and Sips isotherms using the experimental data from the batch experiments. Fitting to the linearized isotherm models was also conducted, however, the nonlinear regression results produced a lower error values and lower  $R^2$  values compared to those provided from the linearized form (data presented in SM, Table SM1). The error functions for the examined isotherm models were computed for further evaluation of the goodness of the fit of the models and the results are presented in Table 3. The use of the linearized form of isotherm models showed that the data of As(III) and As(V) adsorption onto bone char best fitted by the Redlich-Peterson and Langmuir models, respectively. However, the error analysis showed that the nonlinear forms of the models provided more accurate way to calculate the isotherm parameters.

Comparing the data of As(III) adsorption results using two parameters models, the data showed a better fit to the Freundlich model which can be further affirmed by the higher RSQ and lower SNE. In addition, the value of  $1/n$  (1.02) at the lowest error calculated, confirms the favorable adsorption of As(III) on bone char (Table 2). This could be also noticed from the very low value of  $K_L$  presented in Table 2, which refers to a low affinity in the case of the Langmuir model (Li et al., 2008). The value of  $K_L$  in the Langmuir model is correlated to the surface area and pore volume, showing that their increase would result in a higher removal capacity. However, our previous study showed a negative correlation between surface area/pore volume and the removal efficiency (Alkurdi et al., 2020). This may be explained by the results achieved by Samsuri et al. (2013) who examined the removal of As(III) and As(V) using empty fruit bunch and rice husk biochar. Both of the adsorbent removed almost the same amount of As species regardless of the larger surface area of rice husk. The study

alluded to the contribution of some other factors in the removal process such as the point of zero charge and the aromaticity and polarity indices.

Comparing the data of As(III) adsorption fits to the Langmuir and Freundlich models with those of the three parameters models (R-P and Sips models), the data of As(III) removal from aqueous solution best fitted the Sips isotherm model with the lowest SNE value as shown in Table 3. The Sips model fitted the data with  $R^2$  value of 0.999 at an exponent factor of  $n=0.858$ . This result confirms that the removal of As(III) on bone char followed the Freundlich model at the lower concentrations and the Langmuir model when the concentrations were raised. This may be related to the contribution of both the physical and chemical adsorption processes in removal (which may be confirmed by examining the kinetic models).

Fig. 3b shows the plot of the four models for As(V) data along with the experimental data. Similarly, the parameters were calculated using both linearized and nonlinear forms of the models, but the analyses were based on the nonlinear results due to the lower SNE value provided by this form rather than those of the linearized forms. The least fit of the data was with the Freundlich models with either forms; linearized or nonlinearized due to the low  $R^2$  values provided and the higher SNE values calculated. In addition, the value of the  $1/n$  was found to be  $<1$ , referring to an unfavorable adsorption. The Langmuir model constant  $K_L$  was found to be higher for As(V) adsorption than the one calculated for As(III) adsorption (0.114 and 0.009, respectively), which explains the best fit of the data to the Langmuir model. Furthermore, the lowest SNE value (Table 4) was obtained by the Langmuir model with  $R^2$  of 0.977 (Tables 2 and SM1) suggesting a monolayer homogeneous surface coverage of As(V) on bone char (Niazi et al., 2018a). Similar results were reported by Begum et al. (2016) and Liu et al. (2014) for As(V) removal on bone char where the data best fitted the Langmuir model.

### 3.4 Kinetics modelling

Adsorption and desorption are time dependent processes. Thus, the evaluation of the design and the regeneration of an adsorbent requires the determination of the adsorption rate to reach equilibrium (Azizian, 2004). Mathematical models proposed to describe the kinetics process of adsorption can be classified into adsorption diffusion models and adsorption reaction models. Adsorption diffusion models are based on three main steps: external diffusion followed by an internal diffusion or intra-particle diffusion, and finally an exchange process between the adsorbate and the active sites of the adsorbent (Qiu et al., 2009). On the other hand, adsorption reaction models are based on chemical reactions that are not normally considered in adsorption process modelling (Qiu et al., 2009). In this study, some of the widely used batch kinetic models were examined to study the behavior of the bone char as an adsorbent for As species removal from the water.

Examining the suitability of these models to represent the experimental data of the As(III) and As(V) batch experiments was evaluated by determining the parameters of fitting and error function as described earlier. The examination of the goodness of fit applying the linearized forms of the aforementioned kinetic models revealed that these forms do not provide adequate representation of the experimental data confirmed by the value of the errors presented in the SNE calculation tables in most of the fittings (Tables SM2 and SM3). However, the use of nonlinear regression methods had resulted in a deviation of the calculated  $q_e$  values from the experimental with a lower  $R^2$  in some cases. The explanation for these differences was studied and reported by Lin and Wang (2009). The authors reported that using the nonlinear form of the models is much more accurate for two reasons. First, the alteration of a nonlinear form to linear changes the error structure of these functions, and thus the parameters of the models. Second, the use of experimental  $q_e$  to fit the empirical model increased the error of the parameters, while this value is calculated independently from the

mathematical forms in the case of the nonlinear form of the models. Thus, regardless of the lower  $R^2$  value (in some cases), the nonlinear form of the models was presented in the study and the differences were stated in the supplementary materials (Table SM4).

Fig. 4. shows the fitting curves of the kinetic models to the data of As(III). Based on these results, As(III) adsorption onto bone char was found to follow the Pseudo-first-order kinetic model at an initial concentration of 0.5 mg/L with  $R^2=0.996$ . However, increasing the initial concentration to 2.5 and 5 mg/L revealed that the removal kinetic behavior started following the Pseudo-second-order model with  $R^2$  of 0.988 and 0.978, respectively. At 10 mg/L initial concentration, the data were found to best fit the Elovich model due to its very low value of SNE compared to the other models ( $R^2=0.986$ ). This indicates the significant effect of the initial concentration on the rate of As(III) removal on bone char. The parameters that were found to best fit the data (used in Fig. 4) are presented in Table 5.

Table 5 shows the error analysis of the kinetic models for As(III) removal at 0.5 mg/L initial concentration. The results of the same analysis for 2, 5 and 10 mg/L initial concentration are provided in the supplementary materials (Tables SM5-SM7). Given the unavailability of data in the literature pertaining to As(III) removal with bone char, we believe that this study is the first attempt to scrutinize As(III) adsorption onto bone char, and can be used as a base for further investigations.

Similar to As(III), kinetic models of As(V) adsorption onto bone char were examined for an initial concentration of 0.5 mg/L and the results are presented in Table 7. Error analyses were also conducted for the fitted models to help identify the best fit for the experimental data of As(V) adsorption. Fig. 5 shows the data fittings of As(V) using these models. The outcome of the kinetic models fitting of As(V) adsorption with higher initial concentrations is presented in Table 7. The data show that the Pseudo-first-order model produces the best fit for As(V) adsorption with the highest coefficient of determination value and lowest SNE. However,

when raising the initial concentration to 2.5 and 5 mg/L, the Pseudo-second-order model had the best fit for the experimental adsorption data (Table SM8-SM10). While at 10 mg/L the data best fitted the Elovich model indicating a chemical adsorption at higher concentrations. The removal of As(V) on bone char was reported in recent studies to follow the Pseudo-first-order model by Chen et al. (2008) and Pseudo-second-order by Begum et al. (2016) at an initial concentration of 10 mg/L. Furthermore, Liu et al. (2014) reported that the removal of As(V) at 2.5, 5 and 10 mg/L also followed the Pseudo-second-order model. Recent studies for As(V) removal on bone char mostly use the Pseudo-first and second-order models to examine the fit of experimental data. Therefore, the comparison was only made with these two models.

Based on the observations obtained from the kinetic models, both As(III) and As(V) removal followed the PFO model indicating physical adsorption at low concentrations. However, at higher concentrations, Pseudo-second-order and Elovich models provided the best fit the adsorption indicating chemical interaction between bone char and As species.

### 3.4.2 Adsorption diffusion models

The fit of the experimental data to the intraparticle and pore diffusion models is illustrated in Fig. 6 and 7. As(III) plot shows that the linear plot did not pass through the origin which indicated that the intraparticle diffusion was not the only rate controlling step and other factors controlled the removal to some degree. Similar results were achieved when examining the suitability of the Boyd model to fit the data at 0.5, 2.5 and 5 mg/L as the fit of the straight line had a high  $R^2$ . On the other hand, the experimental data at 10 mg/L failed to produce a straight line with an  $R^2$  of 0.87, suggesting the contribution of other diffusion mechanisms at a concentration of 10 mg/L (Fig. 7).

As(V) adsorption onto bone char could also be said to occur due to intraparticle diffusion mechanism as the plot of  $q_t$  versus  $t^{0.5}$  resulted in a linear relationship. However, there seem that two phases of the intraparticle diffusion occurred; low adsorption, represented by the first segment of the fitting line (at time of approximately  $\leq 45$  min), followed by high adsorption beyond 45 min. The fitting lines of the all the concentrations did not pass through zero indicating that the removal of As(V) was not solely due to intraparticle diffusion, but another mechanism would have to be considered. Fig. 7 shows the plot of data after applying the Boyd model for the four concentrations of each As(III) and As(V). Two concentrations are presented on each sub-figure for the sake of clarity as the data interfere with each other when presented together. From Fig. 7, it can be seen that the pore diffusion mechanism might also contribute to the removal process at 0.5 and 2.5 mg/L initial concentration. Raising the initial concentrations to 5 and 10 mg/L reduced the linearity of the fit. This means that at higher concentrations, the pore diffusion mechanism had no contribution to the adsorption process. Similar results were reported by Chen et al. (2008) when examining the mechanism of As(V) removal on bone char at initial concentrations of 0.5, 1, and 1.5 mg/L. Their study confirmed that the removal was complex and due to surface adsorption and the intraparticle diffusion mechanism. Moreover, studying the controlling rate of As(III) and As(V) on graphene showed that the intraparticle and the outer diffusion were both contributing to the adsorption process (Yu et al., 2015). Similarly, the outer diffusion is the controlling mechanism of the removal when the pore diffusion is applicable since the line fittings do not pass through the origin.

#### 4. EDS analysis

The adsorption of As(III) and As(V) onto BC900 was confirmed through EDS analysis as illustrated in Fig. 8. The surface elemental analyses of pristine bone char are in line with those reported in (Rojas-Mayorga et al., 2016) where Ca, P and O being the major elements

of the structure. Comparing the mass percentage of surface elements of BC900 to those loaded with As species, it can be seen from Fig. 8 that there are changes in the elemental composition after adsorption. The main changes occurred due to loading As(III) onto the bone char was due to the reduction in the C, O, Na, Mg and P percentage mass and the appearance of As(III). On the other hand, As(V) affected the content of C, O, Na and Mg. A study conducted by Shakoor et al. (2019) also observed changes in EDS peaks of O, Ca, Na and Mg after the adsorption of As species onto egg shell (resembling structure to bone char) (Katsoyiannis et al., 2015; Tsai et al., 2006). The changes in these elements suggest that the immobilization of As species on bone char was in the form of As oxides and metal complexes (Alkurdi et al., 2020; Cheng et al., 2016). Similar findings were reported by Niazi et. a. (2018) who tested inorganic arsenic species removal with Japanese oak biochar.

## 5. FTIR analysis

The FTIR spectra of As(III) and As(V) loaded bone char revealed a shift in the position of some spectral peaks. Fig. 9 shows the FTIR spectral bands of bone char (red line), As(III) loaded (purple line) and As(V) loaded bone char (green line). The FTIR analysis was used to detect the changes in the bone char structure after loading it with As(III) or As(V). The main changes was in the region of oxygen functional group peaks (OH group at the range of 3303-3690  $\text{cm}^{-1}$  (Amen et al., 2020)) and the 750-1640  $\text{cm}^{-1}$  region which is associated with metal and inorganic complexes formation such as As-Mg and As- $\text{PO}_4$ . The FTIR results match well the EDS analysis where changes in O, P, Mg were detected after the adsorption of As onto bone char. Our results are in agreement with the finding of (Chen et al., 2008) where change in the peak intensity in the region 3303-3690  $\text{cm}^{-1}$  was observed. Chen and co-workers attributed this change to the exchange of OH group on bone char surface with  $\text{HAsO}_4$ . Similarly, (Shakoor et al., 2019) observed changes in FTIR spectra of egg shell after loading it with As (III) and As (V) in 600-1650  $\text{cm}^{-1}$  and 3000-3700  $\text{cm}^{-1}$  regions. From FTIR and

EDS analysis, one can deduce that the main adsorption mechanisms of As species onto bone char are interaction with functional groups and formation of metal complexes.

## 6. Conclusion

The removal of As(III) and As(V) with bone char was thoroughly examined in this study taking into consideration the adsorption kinetics, isotherms and diffusion models. Four isotherm models were tested for each of the As species: Langmuir, Freundlich Redlich-Peterson and Sips models. Similarly, the kinetics were examined using Pseudo-first-order, Pseudo-second-order, Elovich and Ritchie models. Both the linear and nonlinear forms of the models were tested for fitting against the experimental data. Five error functions namely square of the error (SSE), hybrid fractional error function (HYBRID), Marquardt's percent standard deviation (MPSD), average relative error (ARE) and the sum of the absolute error (SAE) were utilized to scrutinize the models' goodness of fit. The results of the fitting for isotherm and kinetic models of As species were found to be different, with a best fit provided by the Sips model for As(III) and the Langmuir model for As(V). On the other hand, the kinetic models were dependent on the initial concentration of As species. At low concentrations of 0.5 mg/L, Pseudo-first-order best described the adsorption kinetics of As species. When higher concentrations tested, Pseudo-second-order and Elovich models provided the best fit for the adsorption experimental data. It was found that at low concentration, intraparticle diffusion and pore diffusion were both effective for As(III) and As(V). However, the pore diffusion model was not suitable for describing adsorption when the initial concentration of As(III) increased beyond 10 mg/L. For As(V) adsorption, fitting against the intraparticle diffusion model exhibited a two-stage linear trend; low adsorption capacity at time  $\leq 45$  min and high adsorption capacity beyond this time. Furthermore, the effect of the pore diffusion model was valid up to 5 mg/L for As(V) adsorption. Structural

analysis using EDS was used to confirm the adsorption of As species by BC900 and examining the changes in the chemical composition of the As loaded samples. FTIR was used to detect the changes in the functional groups and the fingerprint region after adsorption. The results showed that the adsorption of As species onto bone char was possibly due to the formation of As oxides and metal complexes on bone char. For future work recommendations, it would be useful to explore the efficiency of the identified optimum removal parameters for As species in column packed reactors.

### Acknowledgments

This research was performed as a part of PhD research which was supported in part by the Iraqi Government and the Australian Research Training Program.

### References

- Alam, M.A., Shaikh, W.A., Alam, M.O., Bhattacharya, T., Chakraborty, S., Show, B. and Saha, I., 2018. Adsorption of As (III) and As (V) from aqueous solution by modified *Cassia fistula* (golden shower) biochar. *Appl. Water Sci.* 8(7), 198. <https://doi.org/10.1007/s13201-018-0839-y>.
- Alkurdi, S.S., Al-Juboori, R.A., Bundschuh, J., Bowtell, L. and McKnight, S., 2020. Effect of pyrolysis conditions on bone char characterization and its ability for arsenic and fluoride removal. *Environ. Pollut.*, 114221. <https://doi.org/10.1016/j.envpol.2020.114221>.
- Alkurdi, S.S., Al-Juboori, R.A., Bundschuh, J. and Hamawand, I., 2019a. Bone char as a green sorbent for removing health threatening fluoride from drinking water. *Environ. Inter.* 127, 704-719. <https://doi.org/10.1016/j.envint.2019.03.065>.
- Alkurdi, S.S., Herath, I., Bundschuh, J., Al-Juboori, R.A., Vithanage, M. and Mohan, D., 2019b. Biochar versus bone char for a sustainable inorganic arsenic mitigation in

- water: What needs to be done in future research? *Environ. Inter.* 127, 52-69.  
<https://doi.org/10.1016/j.envint.2019.03.012>.
- Amen, R., Bashir, H., Bibi, I., Shaheen, S.M., Niazi, N.K., Shahid, M., Hussain, M.M., Antoniadis, V., Shakoor, M.B., Al-Solaimani, S.G., Wang, H., Bundschuh, J. and Rinklebebk, J., 2020. A critical review on arsenic removal from water using biochar-based sorbents: The significance of modification and redox reactions. *Chem. Eng. J.*, 125195. <https://doi.org/10.1016/j.cej.2020.125195>.
- Amin, A.E.-E.A.Z., 2020. Sulfur, Na<sub>2</sub>-EDTA and their mixture effects on phosphorus release from cow bone char in P-poor sandy soil. *Environ. Technol. Innov.* 17, 100636. <https://doi.org/10.1016/j.eti.2020.100636>.
- Anirudhan, T. and Radhakrishnan, P., 2009. Kinetic and equilibrium modelling of Cadmium (II) ions sorption onto polymerized tamarind fruit shell. *Desalination* 249(3), 1298-1307. <https://doi.org/10.1016/j.desal.2009.06.028>.
- Azizian, S., 2004. Kinetic models of sorption: a theoretical analysis. *J. Colloid. Interface. Sci.* 276(1), 47-52. <https://doi.org/10.1016/j.jcis.2004.03.048>.
- Begum, S.A., Golam Hyder, A. and Vahdat, N., 2016. Adsorption isotherm and kinetic studies of As (V) removal from aqueous solution using cattle bone char. *J. Water Supply Res. T.* 65(3), 244-252. <https://doi.org/10.2166/aqua.2016.089>.
- Chen, Y.-N., Chai, L.-Y. and Shu, Y.-D., 2008. Study of arsenic (V) adsorption on bone char from aqueous solution. *J. Hazard. Mater.* 160(1), 168-172. <https://doi.org/10.1016/j.jhazmat.2008.02.120>.
- Cheng, Z., Fu, F., Dionysiou, D.D. and Tang, B., 2016. Adsorption, oxidation, and reduction behavior of arsenic in the removal of aqueous As (III) by mesoporous Fe/Al bimetallic particles. *Water Res.* 96, 22-31. <https://doi.org/10.1016/j.watres.2016.03.020>.

- Cheung, C., Porter, J. and McKay, G., 2001. Sorption kinetic analysis for the removal of cadmium ions from effluents using bone char. *Water Res.* 35(3), 605-612. [https://doi.org/10.1016/S0043-1354\(00\)00306-7](https://doi.org/10.1016/S0043-1354(00)00306-7).
- Cheung, C.W., Porter, J.F. and McKay, G., 2000. Elovich equation and modified second-order equation for sorption of cadmium ions onto bone char. *J. Chem. Technol. Biotechnol.* 75(11), 963-970.
- Czerniczyniec, M., Fariás, S., Magallanes, J. and Cicerone, D., 2007. Arsenic (V) adsorption onto biogenic hydroxyapatite: solution composition effects. *Water Air Soil Pollut.* 180(1-4), 75-82. <https://doi.org/10.1007/s11270-006-9251-6>.
- Darvishi Cheshmeh Soltani, R., Safari, M., Maleki, A., Rezaee, R., Shahmoradi, B., Shahmohammadi, S. and Ghahramani, E., 2017. Decontamination of arsenic(V)-contained liquid phase utilizing Fe<sub>3</sub>O<sub>4</sub>/bone char nanocomposite encapsulated in chitosan biopolymer. *Environ. Sci. Pollut. Res.* 24(17), 15157-15166. <https://doi.org/10.1007/s11356-017-9128-9>.
- Dieme, M., Villot, A., Gerente, C., Andres, Y., Diop, S. and Diawara, C., 2017. Sustainable conversion of agriculture wastes into activated carbons: energy balance and arsenic removal from water. *Environ. Technol.* 38(3), 353-360. <https://doi.org/10.1080/09593330.2016.1193225>.
- El-Khaiary, M.I. and Malash, G.F., 2011. Common data analysis errors in batch adsorption studies. *Hydrometallurgy* 105(3-4), 314-320. <https://doi.org/10.1016/j.hydromet.2010.11.005>.
- Ermolenko, A., Shevelev, A., Vikulova, M., Blagova, T., Altukhov, S., Gorokhovskiy, A., Godymchuk, A., Burmistrov, I. and Ofor, P.O., 2020. Wastewater treatment from lead and strontium by potassium polytitanates: Kinetic analysis and adsorption mechanism. *Processes* 8(2), 217. <https://doi.org/10.3390/pr8020217>.

- Hashim, M.A., Kundu, A., Mukherjee, S., Ng, Y.-S., Mukhopadhyay, S., Redzwan, G. and Gupta, B.S., 2019. Arsenic removal by adsorption on activated carbon in a rotating packed bed. *J. Water Process. Eng.* 30, 100591. <https://doi.org/10.1016/j.jwpe.2018.03.006>.
- Herath, I., Vithanage, M., Bundschuh, J., Maity, J.P. and Bhattacharya, P., 2016. Natural Arsenic in Global Groundwaters: Distribution and Geochemical Triggers for Mobilization. *Curr. Pollut. Rep.* 2(1), 68-89.
- Ho, Y.-S., 2006. Review of second-order models for adsorption systems. *J. Hazard. Mater.* 136(3), 681-689. <https://doi.org/10.1016/j.jhazmat.2005.12.043>.
- Ho, Y., Porter, J. and McKay, G., 2002. Equilibrium isotherm studies for the sorption of divalent metal ions onto peat: copper, nickel and lead single component systems. *Water Air Soil Pollut.* 141(1-4), 1-33. <https://link.springer.com/article/10.1023/A:1021304828010>.
- Kalaruban, M., Loganathan, P., Nguyen, T.V., Nur, T., Johir, M.A.H., Nguyen, T.H., Trinh, M.V. and Vigneswaran, S., 2019. Iron-impregnated granular activated carbon for arsenic removal: application to practical column filters. *J. Environ. Manage.* 239, 235-243. <https://doi.org/10.1016/j.jenvman.2019.03.053>.
- Katsoyiannis, I.A., Mitrakas, M. and Zouboulis, A.I., 2015. Arsenic occurrence in Europe: Emphasis in Greece and description of the applied full-scale treatment plants. *Desalination Water Treat.* 54(8), 2100-2107. <https://doi.org/10.1080/19443994.2014.933630>.
- Kumar, M. and Ramanathan, A. 2019. Arsenic speciation of groundwater and agricultural soils in central Gangetic basin, India, p. 225, CRC Press.
- Kumara, N., Hamdan, N., Petra, M.I., Tennakoon, K.U. and Ekanayake, P., 2014. Equilibrium isotherm studies of adsorption of pigments extracted from kuduk-kuduk

- (*Melastoma malabathricum* L.) pulp onto TiO<sub>2</sub> nanoparticles. *J. Chem.* 2014. <https://doi.org/10.1155/2014/468975>.
- Kumarathilaka, P., Seneweera, S., Ok, Y.S., Meharg, A.A. and Bundschuh, J., 2020. Mitigation of arsenic accumulation in rice: An agronomical, physico-chemical, and biological approach—A critical review. *Crit. Rev. Environ. Sci. Technol.* 50(1), 31-71. <https://doi.org/10.1080/10643389.2019.1618691>.
- Li, G.-Y., Jiang, Y.-R., Huang, K.-L., Ding, P. and Yao, L.-L., 2008. Kinetics of adsorption of *Saccharomyces cerevisiae* mandelated dehydrogenase on magnetic Fe<sub>3</sub>O<sub>4</sub>–chitosan nanoparticles. *Colloids Surf. A Physicochem. Eng. Asp.* 320(1-3), 11-18. <https://doi.org/10.1016/j.colsurfa.2008.01.017>.
- Lin, J. and Wang, L., 2009. Comparison between linear and non-linear forms of pseudo-first-order and pseudo-second-order adsorption kinetic models for the removal of methylene blue by activated carbon. *Front Environ. Sci. Eng.* 3(3), 320-324.
- Liu, B., Kim, K.-H., Kumar, V. and Kim, S., 2020. A review of functional sorbents for adsorptive removal of arsenic ions in aqueous systems. *J. Hazard. Mater.* 388, 121815. <https://doi.org/10.1016/j.jhazmat.2019.121815>.
- Liu, J., Huang, X., Liu, J., Wang, W., Zhang, W. and Dong, F., 2014. Adsorption of arsenic (V) on bone char: batch, column and modeling studies. *Environ. Earth Sci.* 72(6), 2081-2090.
- Malash, G.F. and El-Khaiary, M.I., 2010. Piecewise linear regression: A statistical method for the analysis of experimental adsorption data by the intraparticle-diffusion models. *Chem. Eng. J.* 163(3), 256-263. <https://doi.org/10.1016/j.cej.2010.07.059>.
- Meher, A., Pillewan, P., Rayalu, S. and Bansawal, A., 2016. Arsenic removal from water using metal and metal oxide modified zeolites. *Arsen. Res. Glob. Sustain.*, 482-483.

- Minja, R.J., 2020. Practical Approach for Removal of Natural Organic Matter and Defluoridation of Maji ya Chai River Water: Use of Acid Pre-treated Bone Char and Coagulants. *Tanz. J. Engrg. Technol.* 38(2).
- Mondal, P. and George, S., 2015. A review on adsorbents used for defluoridation of drinking water. *Rev. Environ. Sci. Bio.* 14(2), 195-210.
- Mukherjee, A., Sengupta, M.K., Hossain, M.A., Ahamed, S., Das, B., Nayak, B., Lodh, D., Rahman, M.M. and Chakraborti, D., 2006. Arsenic contamination in groundwater: a global perspective with emphasis on the Asian scenario. *JHPN*, 142-163.
- Niazi, N.K., Bibi, I., Shahid, M., Ok, Y.S., Burton, E.D., Wang, H., Shaheen, S.M., Rinklebe, J. and Lüttge, A., 2018a. Arsenic removal by perilla leaf biochar in aqueous solutions and groundwater: an integrated spectroscopic and microscopic examination. *Environ. Pollut.* 232, 31-41.
- Niazi, N.K., Bibi, I., Shahid, M., Ok, Y.S., Shaheen, S.M., Rinklebe, J., Wang, H., Murtaza, B., Islam, E., Nawaz, M.F. and Lüttge, A., 2018b. Arsenic removal by Japanese oak wood biochar in aqueous solutions and well water: Investigating arsenic fate using integrated spectroscopic and microscopic techniques. *Sci. Total Environ.* 621, 1642-1651. <https://doi.org/10.1016/j.scitotenv.2017.10.063>.
- Nicomel, N.R., Leus, K., Folens, K., Van Der Voort, P. and Du Laing, G., 2016. Technologies for arsenic removal from water: current status and future perspectives. *Int. J. Environ. Res. Public Health* 13(1), 62. <https://doi.org/10.3390/ijerph13010062>.
- Nigri, E.M., Santos, A.L., Bhatnagar, A. and Rocha, S.D., 2019. Chemical regeneration of bone char associated with a continuous system for defluoridation of water. *Braz. J. Chem. Eng.* 36(4), 1631-1643. <https://doi.org/10.1590/0104-6632.20190364s20180258>

- Qiu, H., Lv, L., Pan, B.-c., Zhang, Q.-j., Zhang, W.-m. and Zhang, Q.-x., 2009. Critical review in adsorption kinetic models. *J. Zhejiang Univ. Sci. A* 10(5), 716-724.
- Ramsey, A.C., Duff, E., Paterson, L. and Stuart, J., 1973. The Uptake of F<sup>-</sup> by Hydroxyapatite at Varying pH. *Caries research* 7(3), 231-244.
- Rojas-Mayorga, C.K., Mendoza-Castillo, D.I., Bonilla-Petriciolet, A. and Silvestre-Albero, J., 2016. Tailoring the adsorption behavior of bone char for heavy metal removal from aqueous solution. *Adsorpt. Sci. Technol.* 34(6), 368-387. <https://doi.org/10.1177%2F0263617416658891>.
- Roy, S., 2018. Synthesis of graphene oxide using tea-waste biochar as green substitute of graphite and its application in de-fluoridation of contaminated water. *Am. J. Chem. Res.* 1(1), 1-19.
- Samsuri, A.W., Sadegh-Zadeh, F. and Seh-Bardan, B.J., 2013. Adsorption of As (III) and As (V) by Fe coated biochars and biochars produced from empty fruit bunch and rice husk. *J. Environ. Chem. Eng.* 1(4), 981-988. <https://doi.org/10.1016/j.jece.2013.08.009>.
- Shaheen, S.M., Niazi, N.K., Hassan, N.E., Bibi, I., Wang, H., Tsang, D.C., Ok, Y.S., Bolan, N. and Rinklebe, J., 2019. Wood-based biochar for the removal of potentially toxic elements in water and wastewater: a critical review. *Int. Mater. Rev.* 64(4), 216-247. <https://doi.org/10.1080/09506608.2018.1473096>.
- Shakoor, M.B., Niazi, N.K., Bibi, I., Shahid, M., Saqib, Z.A., Nawaz, M.F., Shaheen, S.M., Wang, H., Tsang, D.C., Bundschuh, J., Ok, Y.S. and Rinklebe, J., 2019. Exploring the arsenic removal potential of various biosorbents from water. *Environ. Inter.* 123, 567-579. <https://doi.org/10.1016/j.envint.2018.12.049>.
- Singh, P. and Mohan, D. 2020. Rice-husk and wheat-husk iron oxide biochar nanocomposites for the sustainable removal of arsenic from water, p. 30.

- Soni, R. and Shukla, D.P., 2019. Synthesis of fly ash based zeolite-reduced graphene oxide composite and its evaluation as an adsorbent for arsenic removal. *Chemosphere* 219, 504-509. <https://doi.org/10.1016/j.chemosphere.2018.11.203>.
- Tabassum, R.A., Shahid, M., Niazi, N.K., Dumat, C., Zhang, Y., Imran, M., Bakhat, H.F., Hussain, I. and Khalid, S., 2019. Arsenic removal from aqueous solutions and groundwater using agricultural biowastes-derived biosorbents and biochar: a column-scale investigation. *Int. J. Phytoremediation* 21(6), 509-518. <https://doi.org/10.1080/15226514.2018.1501340>.
- Tan, K. and Hameed, B., 2017. Insight into the adsorption kinetics models for the removal of contaminants from aqueous solutions. *J. Taiwan Inst. Chem. Eng.* 74, 25-48. <https://doi.org/10.1016/j.jtice.2017.01.024>.
- Tsai, W., Yang, J., Lai, C., Cheng, Y., Lin, C. and Yeh, C., 2006. Characterization and adsorption properties of eggshells and eggshell membrane. *Bioresour. Technol.* 97(3), 488-493. <https://doi.org/10.1016/j.biortech.2005.02.050>.
- Valderrama, C., Gamisans, X., De las Heras, X., Farran, A. and Cortina, J., 2008. Sorption kinetics of polycyclic aromatic hydrocarbons removal using granular activated carbon: intraparticle diffusion coefficients. *J. Hazard. Mater.* 157(2-3), 386-396. <https://doi.org/10.1016/j.jhazmat.2007.12.119>.
- Wang, J. and Guo, X., 2020. Adsorption isotherm models: Classification, physical meaning, application and solving method. *Chemosphere*, 127279. <https://doi.org/10.1016/j.chemosphere.2020.127279>.
- WHO, G., 2011. Guidelines for drinking-water quality. *World Health Organization* 216, 303-304.
- Yadav, S.K., Ramanathan, A., Kumar, M., Chidambaram, S., Gautam, Y. and Tiwari, C., 2020. Assessment of arsenic and uranium co-occurrences in groundwater of central

Gangetic Plain, Uttar Pradesh, India. *Environ. Earth Sci.* 79(6), 1-14.  
<https://doi.org/10.1007/s12665-020-8892-x>.

Yu, F., Sun, S., Ma, J. and Han, S., 2015. Enhanced removal performance of arsenate and arsenite by magnetic graphene oxide with high iron oxide loading. *Phys. Chem. Chem. Phys.* 17(6), 4388-4397. <https://doi.org/10.1039/C4CP04835K>.

Zeltner, W.A. 2002. Simultaneous Removal of Arsenite As (III) and Arsenate As (V) From Drinking Water Using a Novel Photoactive Adsorbent, EPA.

Journal Pre-proof

## Figures

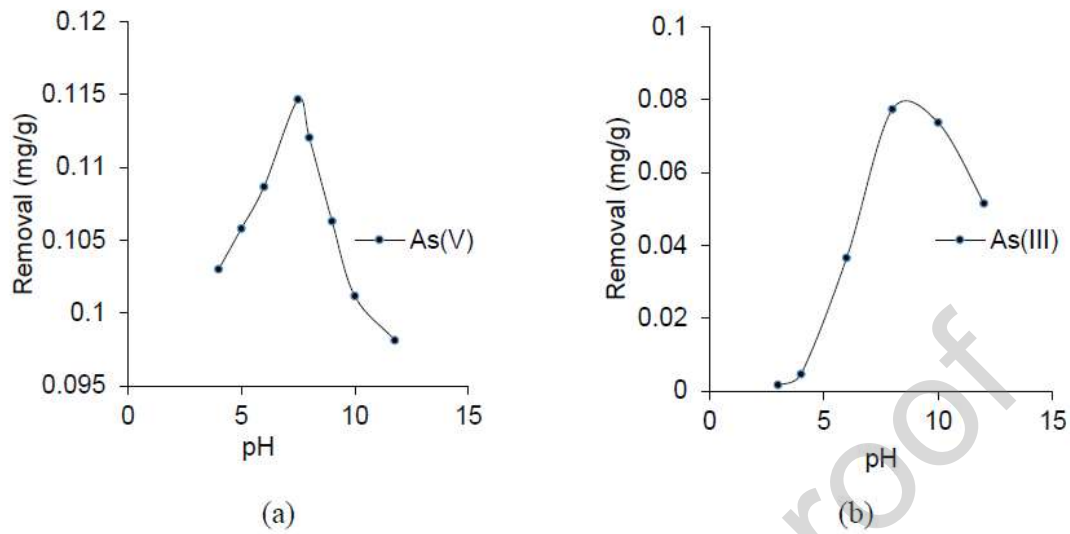


**Fig. 1.** The effect of solution pH on the removal capacity of 1 mg/L (a) As(V) and (b) As(III) using 5 g/L BC900.

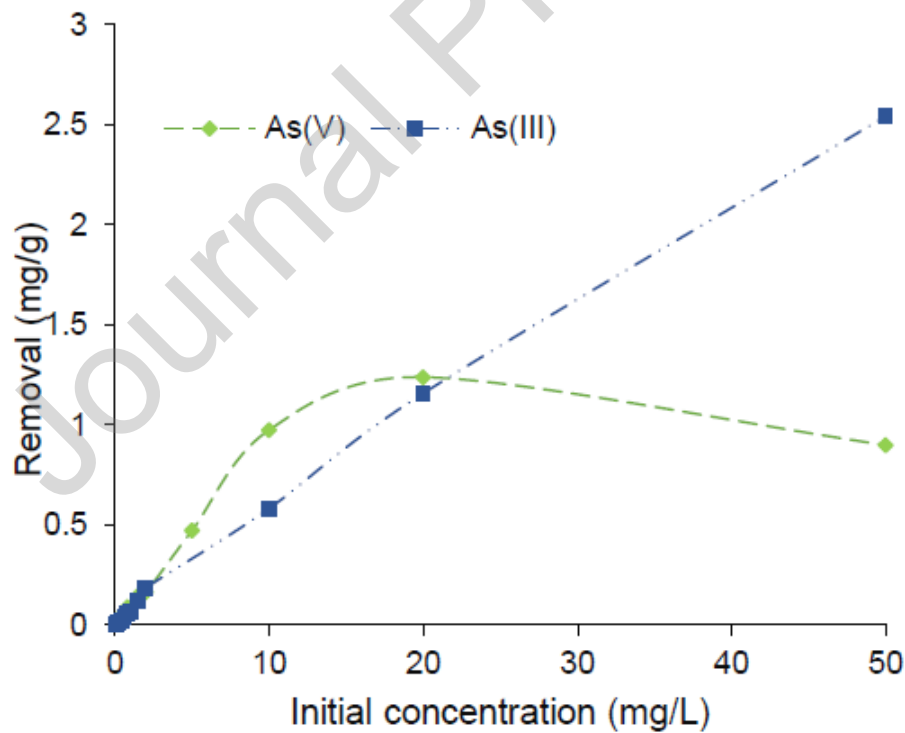
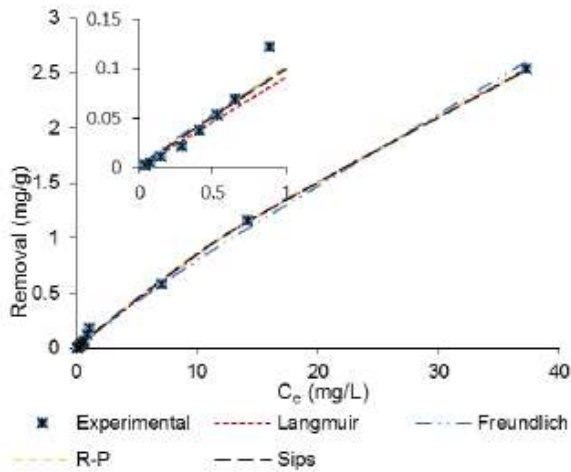
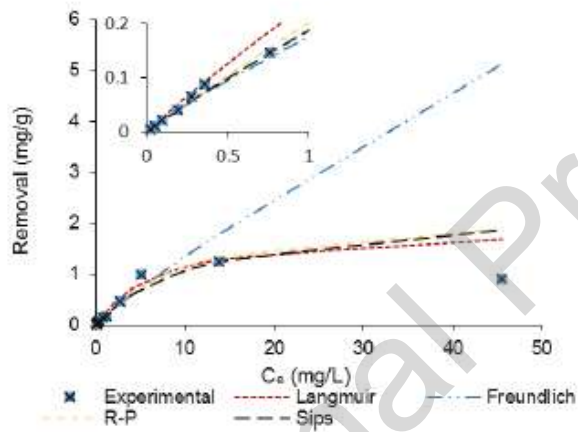


**Fig. 2.** Effect of initial concentration of As(III) and As(V) on removal capacity using 5 g/L BC900 at pH 8.6 and 7.5, respectively.



(a) Plot of isotherm models for As(III)



(b) Plot of isotherm models for As(V)

**Fig. 3.** Isotherm models fit for the experimental data of (a) As(III) and (b) As(V) using 5 g/L BC900 at pH 8.3 and 7.5, respectively.

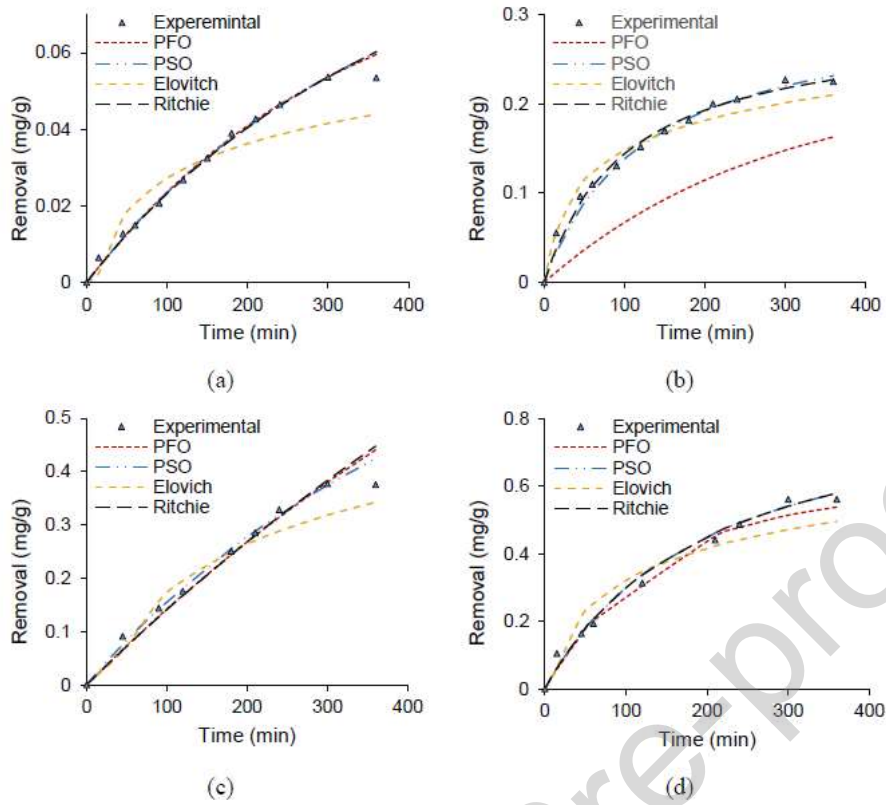


**Fig. 4.** Fitting of the kinetic models and the experimental data for As(III) at an initial concentration of (a) 0.5 mg/L, (b) 2.5 mg/L, (c) 5 mg/L and (d) 10 mg/L using 5 g/L BC900 at pH 8.3.

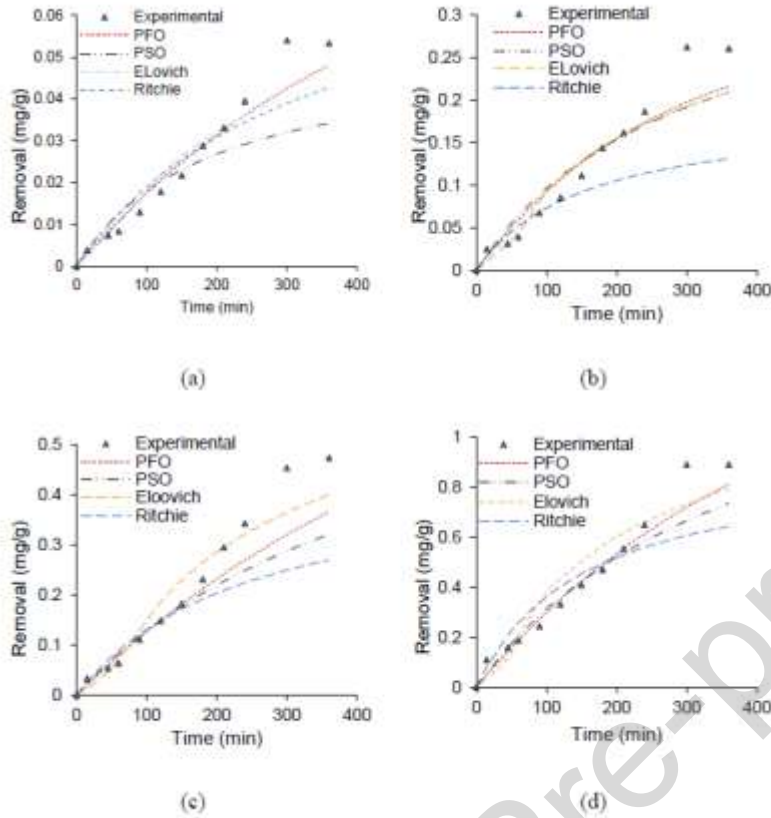


**Fig. 5.** Fitting of the kinetic models of As(V) removal on bone char to the experimental data at (a) 0.5 mg/L, (b) 2.5 mg/L, (c) 5 mg/L and (d) 10 mg/L using 5 g/L BC900 at pH 7.5.

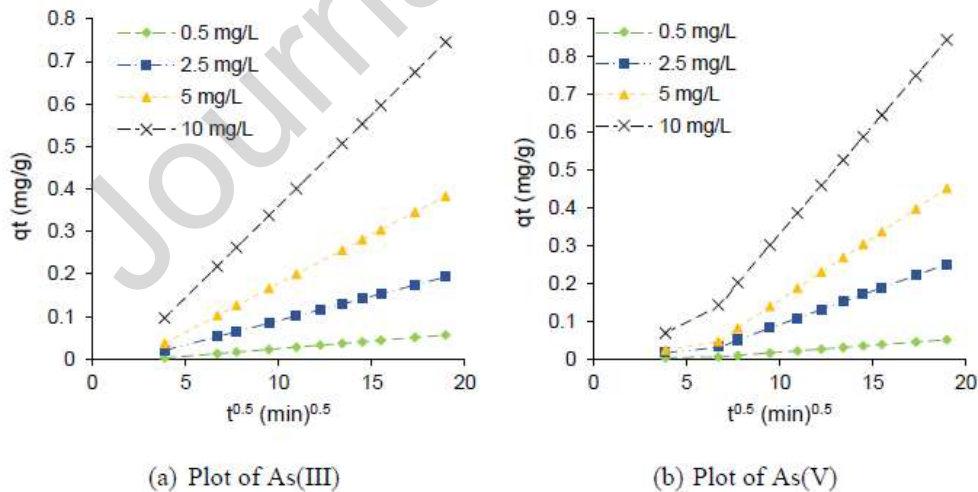
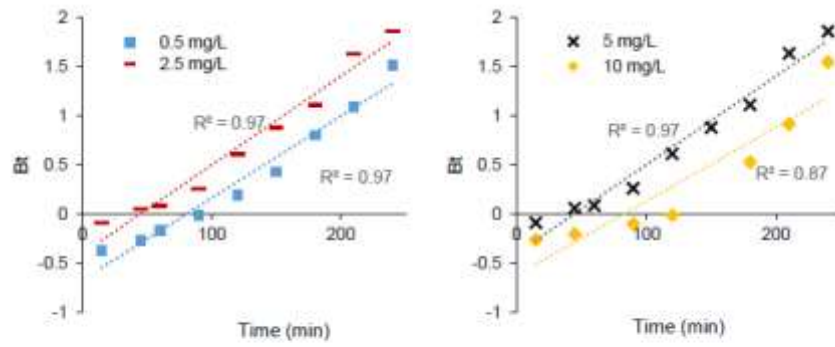
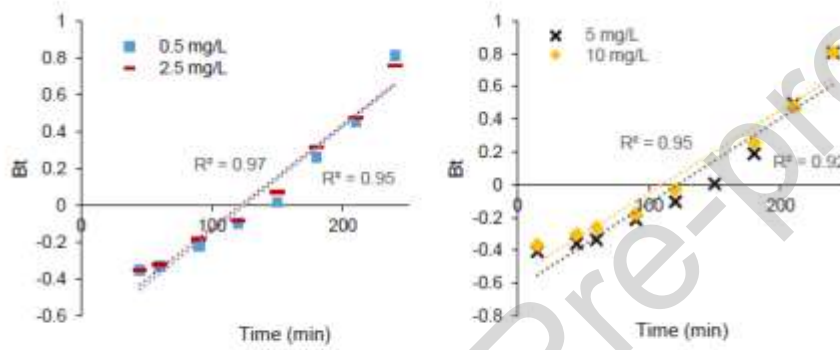


**Fig. 6.** Plot of intra particle diffusion model for (a) As(III) and (b) As(V) experimental data using 5 g/L BC900 at pH 8.6 and 7.5, respectively.

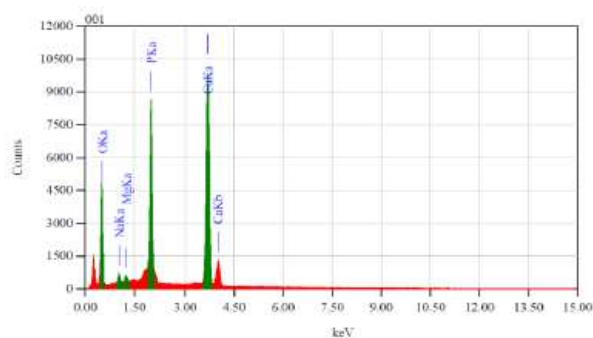


(a) Data plot for As(III) at 0.5, 2.5, 5 and 10 mg/L



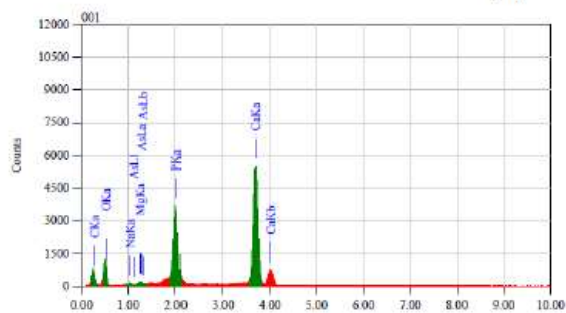
(b) Data plot for As(V) at 0.5, 2.5, 5 and 10 mg/L

**Fig. 7.** Plot of the Boyd model for different concentration of (a) As(III) and (b) As(V) experimental data using 5 g/L bone char at pH 8.6 and 7.5, respectively.



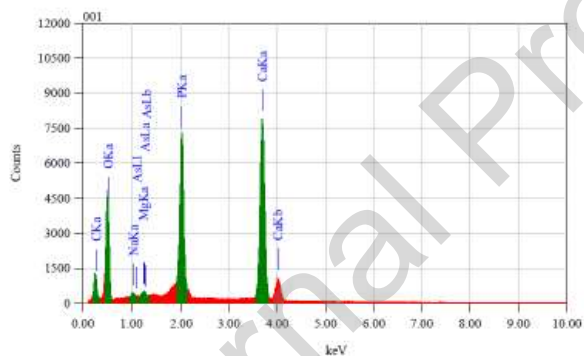
Elements	Mass %
C	3.07
O	38.15
Ca	38.03
P	19.7
Mg	0.66
Na	0.42

(a)



Elements	Mass %
C	3.01
O	38.08
Ca	42.11
P	16.24
Mg	0.35
Na	0.19
As	0.03

(b)



Elements	Mass %
C	2.85
O	40.17
Ca	36.69
P	19.48
Mg	0.30
Na	0.31
As	0.20

(c)

**Fig. 8.** EDS analyses for (a) BC900, (b) As(III) and (c) As(V).

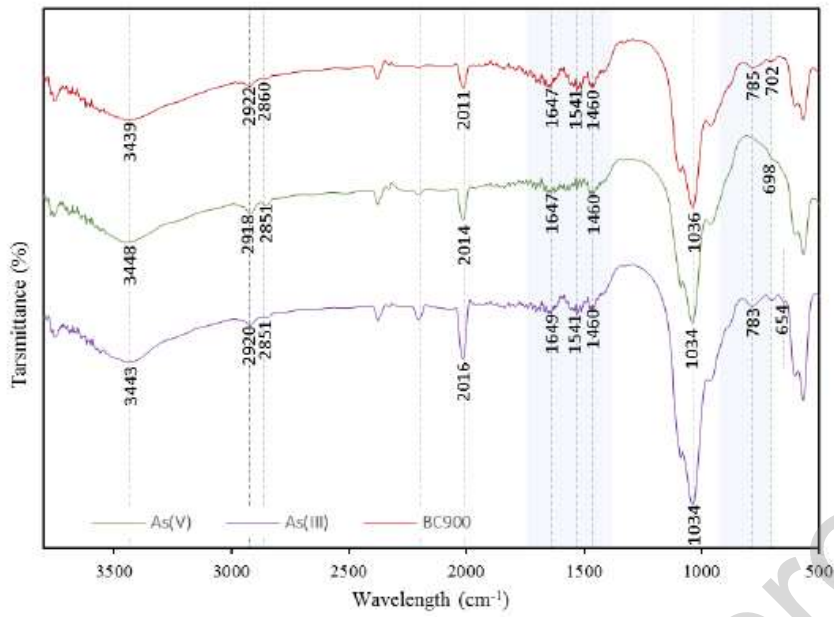


**Fig. 9.** FTIR analysis for As-loaded and unloaded BC900 (Alkurdi et al., 2020).

**Table 1.** Characteristics of bone char.

Charring temperature (°C)	900
Surface pH	11.64
Point of zero charge	8.3
Surface acid groups (mmol/g)	3.526
Surface basic groups (mmol/g)	2.382
Surface area	69.063 m <sup>2</sup> /g
Pore volume	0.235 cm <sup>3</sup> /g
Pore size	13.588 nm

**Table 2.** Parameters of isotherm models for As(III) and As(V) adsorption onto bone char based on the error function calculation from nonlinear regression fitting.

	2-Parameters			3-Parameters			
	Freundlich			Redlich-Peterson			
	$K_F$	$1/n$	$R^2$	$K_{RP}$	$a_{RP}$	$\beta$	$R^2$
As(V)	0.189	0.939	0.888	0.220	0.095	1	0.969
As(III)	0.100	1.0204	0.998	0.113	0.102	0.517	0.999
	Langmuir			Sips			
	$K_L$	$Q_o$	$R^2$	$q_m$	$b$	$n$	$R^2$
	$K_L$	$Q_o$	$R^2$	$q_m$	$b$	$n$	$R^2$
As(V)	0.114	2.042	0.969	2.453	0.083	1.000	0.964
As(III)	0.009	9.822	0.999	2.659	0.040	0.858	0.999

**Table 3.** Error analysis comparison for As(III) isotherm parameters.

	Langmuir isotherm				
	SSE	HYBRID	MPSD	ARE	SAE
$Q_o$	9.822	8.305	21.379	21.379	21.375
$K_L$	0.009	0.012	0.004	0.004	0.004
RSQ	0.999	0.998	0.997	0.997	<b>0.997</b>
SSE	<b>0.010</b>	0.0121	0.029	0.027	0.028
HYBRID	0.601	<b>0.576</b>	0.873	0.9990	1.025
MPSD	30.341	33.077	<b>27.739</b>	28.104	28.200
ARE	20.533	22.656	19.544	<b>19.437</b>	19.517
SAE	0.187	0.245	0.375	0.353	<b>0.351</b>

SNE	<b>3.255</b>	3.626	4.553	4.530	4.605
Freundlich isotherm					
	SSE	HYBRID	MPSD	ARE	SAE
$K_F$	0.119	0.100	0.080	0.078	0.102
1/n	0.847	1.020	0.900	1.015	0.889
RSQ	0.999	0.998	0.993	0.993	0.998
SSE	<b>0.008</b>	0.015	0.473	0.302	0.008
HYBRID	0.970	<b>0.651</b>	2.631	1.997	1.013
MPSD	103.619	60.693	<b>27.569</b>	27.721	106.656
ARE	62.579	37.178	19.592	<b>19.200</b>	64.324
SAE	0.245	0.245	0.245	0.245	<b>0.245</b>
SNE	3.329	<b>2.427</b>	3.563	2.956	3.401
Redlich-Peterson isotherm					
	SSE	HYBRID	MPSD	ARE	SAE
$K_{RP}$	0.189	0.113	0.081	0.081	0.081
$a_{RP}$	0.679	0.102	0.004	0.005	0.005
$\beta$	0.265	0.517	1.000	1.000	1.000
RSQ	0.999	0.999	0.997	0.998	0.998
SSE	<b>0.008</b>	0.009	0.029	0.019	0.019
HYBRID	0.716	<b>0.573</b>	0.970	0.950	0.950
MPSD	73.772	45.273	<b>29.239</b>	29.288	29.288
ARE	44.370	27.996	19.544	<b>19.409</b>	19.409
SAE	0.219	0.196	0.375	0.288	<b>0.288</b>
SNE	3.587	<b>2.655</b>	3.839	3.243	3.244
Sips isotherm					

	SSE	HYBRID	MPSD	ARE	SAE
$q_m$	2.659	8.305	9.822	1.957	4.729
b	0.040	0.012	0.040	0.061	0.010
n	0.858	1.000	1.000	0.824	0.768
RSQ	0.999	0.998	0.960	0.922	0.997
SSE	<b>0.010</b>	0.012	0.399	0.884	0.028
HYBRID	0.668	<b>0.640</b>	2.617	4.684	2.415
MPSD	31.982	34.866	<b>21.298</b>	21.895	63.380
ARE	20.533	22.656	14.068	<b>12.988</b>	47.855
SAE	0.187	0.245	0.978	1.227	<b>0.372</b>
SNE	<b>1.240</b>	1.373	2.438	3.617	2.851

**Table 4.** Error analysis comparison for As(V) isotherm parameters.

Langmuir isotherm					
	SSE	HYBRID	MPSD	ARE	SAE
$Q_0$	1.961	2.042	2.217	2.042	2.313
$K_L$	0.138	0.114	0.098	0.114	0.095
RSQ	0.977	0.969	0.969	0.974	0.974
SSE	<b>0.104</b>	0.143	0.227	0.991	0.155
HYBRID	5.126	<b>1.888</b>	2.510	9.158	2.230
MPSD	153.069	39.166	<b>20.556</b>	30.398	50.690
ARE	99.622	27.041	16.567	<b>15.42</b>	32.492
SAE	0.758	0.659	0.827	1.171	<b>0.568</b>
SNE	3.312	<b>1.440</b>	1.510	3.353	1.543

Freundlich isotherm					
	SSE	HYBRID	MPSD	ARE	SAE
$K_F$	0.251	0.182	0.164	0.189	0.179
$1/n$	0.637	0.779	0.866	0.939	0.736
RSQ	0.906	0.913	0.905	0.888	0.932
SSE	<b>0.045</b>	0.057	0.061	0.055	0.055
HYBRID	1.396	<b>0.948</b>	0.976	1.010	1.010
MPSD	28.843	17.715	<b>17.536</b>	18.912	18.912
ARE	19.733	11.127	11.303	<b>10.693</b>	10.693
SAE	0.440	0.406	0.385	0.344	<b>0.348</b>
SNE	4.733	3.704	3.7545	<b>3.596</b>	3.596
Redlich-Peterson isotherm					
	SSE	HYBRID	MPSD	ARE	SAE
$K_{RP}$	0.271	0.220	0.242	0.245	0.245
$a_{RP}$	0.138	0.095	0.297	0.322	0.322
$\beta$	1.000	1.000	0.612	0.645	0.642
RSQ	0.977	0.969	0.947	0.953	0.953
SSE	<b>0.045</b>	0.057	0.101	0.109	0.109
HYBRID	1.570	<b>1.067</b>	1.511	1.650	1.649
MPSD	30.593	18.790	<b>17.655</b>	18.001	18.008
ARE	19.733	11.127	11.272	<b>10.733</b>	10.733
SAE	0.440	0.402	0.529	0.460	<b>0.460</b>
SNE	4.196	<b>3.109</b>	3.991	4.003	4.003
Sips isotherm					
	SSE	HYBRID	MPSD	ARE	SAE

$q_m$	1.373	1.897	2.982	2.453	2.453
b	0.120	0.117	0.067	0.083	0.083
n	0.581	0.897	0.995	1.0	0.997
RSQ	0.992	0.978	0.957	0.964	0.964
SSE	<b>0.018</b>	0.041	0.082	0.084	0.084
HYBRID	2.046	<b>0.979</b>	1.269	1.324	1.324
MPSD	73.059	28.991	<b>17.313</b>	17.548	17.548
ARE	51.181	20.803	10.982	<b>10.345</b>	10.345
SAE	0.389	0.380	0.476	0.407	<b>0.407</b>
SNE	4.817	3.065	3.036	<b>2.915</b>	2.915

**Table 5.** Kinetic models' parameters for As(III) adsorption onto bone char from nonlinear regression.

Conc. (mg/L)	PFO			PSO		
	$k_1$	$q_e$	$R^2$	$k_2$	$q_e$	$R^2$
0.5	0.001	0.345	0.996	0.012	0.152	0.992
2.5	0.010	0.226	0.963	0.059	0.247	0.988
5.0	0.001	1.261	0.973	0.001	1.258	0.978
10.0	0.007	0.583	0.979	0.006	0.904	0.983

	Elovich			Sips		
	$\alpha$	$\beta$	$R^2$	$k_2$	$q_e$	$R^2$
0.5	0.001	76.623	0.858	0.002	0.156	0.996
2.5	0.009	18.592	0.976	0.292	0.010	0.956
5.0	0.005	7.460	0.975	0.001	0.954	0.971

10.0                    0.015   7.368   0.986                    0.005   0.904   0.983

**Table 6.** Error analysis for kinetic models of As(III) adsorption onto bone char.

Pseudo-first-order (PFO)					
	SSE	HYBRID	MPSD	ARE	SAE
$q_e$	0.345	0.089	0.075	0.096	0.096
$k_1$	0.001	0.003	0.004	0.003	0.003
RSQ	0.997	0.996	0.993	0.997	0.992
SSE	<b>0.0001</b>	0.000	0.000	0.000	0.000
HYBRID	0.044	<b>0.014</b>	0.016	0.015	0.015
MPSD	20.747	13.933	<b>13.571</b>	14.525	14.525
ARE	12.582	5.767	7.552	<b>5.507</b>	5.507
SAE	0.023	0.007	0.013	0.007	<b>0.007</b>
SNE	5.000	<b>1.903</b>	2.456	1.925	1.925
Pseudo-second-order (PSO)					
	SSE	HYBRID	MPSD	ARE	SAE
$q_e$	0.302	0.140	0.101	0.152	0.152
$k_2$	0.003	0.015	0.033	0.012	0.012
RSQ	0.996	0.995	0.986	0.992	0.996
SSE	<b>3.1E-05</b>	9.9E-06	3.5E-05	9.6E-06	9.6E-06
HYBRID	0.030	<b>0.014</b>	0.021	0.015	0.015
MPSD	18.798	13.822	<b>12.739</b>	14.543	14.543
ARE	9.5541	6.0720	8.5852	<b>5.5367</b>	5.5367
SAE	0.0148	0.0075	0.0168	0.0063	<b>0.0063</b>
SNE	4.776	2.573	4.287	<b>2.498</b>	2.498

Elovich					
	SSE	HYBRID	MPSD	ARE	SAE
$\alpha$	0.001	0.001	0.001	0.001	0.001
$\beta$	60.636	76.623	100.317	102.173	49.128
RSQ	0.975	0.975	0.975	0.975	0.975
SSE	<b>0.0003</b>	0.0004	0.001	0.001	0.0004
HYBRID	0.264	<b>0.185</b>	0.258	0.253	0.656
MPSD	55.860	35.724	<b>29.991</b>	31.699	98.657
ARE	30.157	25.422	24.049	<b>22.715</b>	34.526
SAE	0.046	0.054	0.072	0.068	<b>0.037</b>
SNE	2.805	<b>2.585</b>	3.393	3.209	3.994
Ritchie					
	SSE	HYBRID	MPSD	ARE	SAE
$q_e$	0.268	0.149	0.122	0.156	0.156
$K_R$	0.001	0.002	0.003	0.002	0.002
RSQ	0.996	0.996	0.993	0.996	0.996
SSE	<b>2.9E-05</b>	10E-06	1.9E-05	1.1E-05	1.1E-05
HYBRID	0.026	<b>0.014</b>	0.0159	0.014	0.014
MPSD	17.539	13.653	<b>13.265</b>	14.017	14.017
ARE	9.046	5.914	7.640	<b>5.590</b>	5.590
SAE	0.015	0.007	0.013	0.007	<b>0.007</b>
SNE	5.000	2.801	3.738	<b>2.797</b>	<b>2.797</b>

**Table 7.** Kinetic models' parameters for As(V) adsorption onto bone char based on the nonlinear form of the model.

Conc. (mg/L)	PFO			PSO		
	$k_1$	$q_e$	$R^2$	$k_2$	$q_e$	$R^2$
0.5	0.002	0.087	0.963	0.104	0.048	0.878
2.5	0.100	0.228	0.942	0.059	0.247	0.988
5.0	0.001	0.261	0.973	0.001	1.258	0.978
10.0	0.003	1.191	0.922	0.003	1.134	0.903

	Elovich			Sips		
	$\alpha$	$\beta$	$R^2$	$k_2$	$q_e$	$R^2$
0.5	49E-7	43.544	0.945	0.004	0.062	0.896
2.5	0.009	18.592	0.976	0.100	0.292	0.956
5.0	0.005	7.460	0.975	0.001	0.954	0.971
10.0	0.015	7.368	0.986	0.005	0.904	0.983

**Table 8.** Error analysis for kinetic models of As(V) adsorption onto bone char at an initial concentration of 0.5 mg/L.

	Pseudo-first-order (PFO)				
	SSE	HYBRID	MPSD	ARE	SAE
$q_e$	0.065	0.072	0.079	0.079	0.087
$k_1$	0.004	0.003	0.002	0.002	0.002
RSQ	0.945	0.956	0.963	0.964	0.963
SSE	<b>0.0002</b>	0.0002	0.0003	0.000	0.0002
HYBRID	0.111	<b>0.078</b>	0.084	0.098	0.064

MPSD	26.718	18.177	<b>14.951</b>	15.351	17.739
ARE	19.018	13.417	10.432	<b>9.874</b>	12.564
SAE	0.036	0.032	0.033	0.035	<b>0.028</b>
SNE	4.629	3.642	3.627	3.930	<b>3.148</b>

## Pseudo-second-order (PSO)

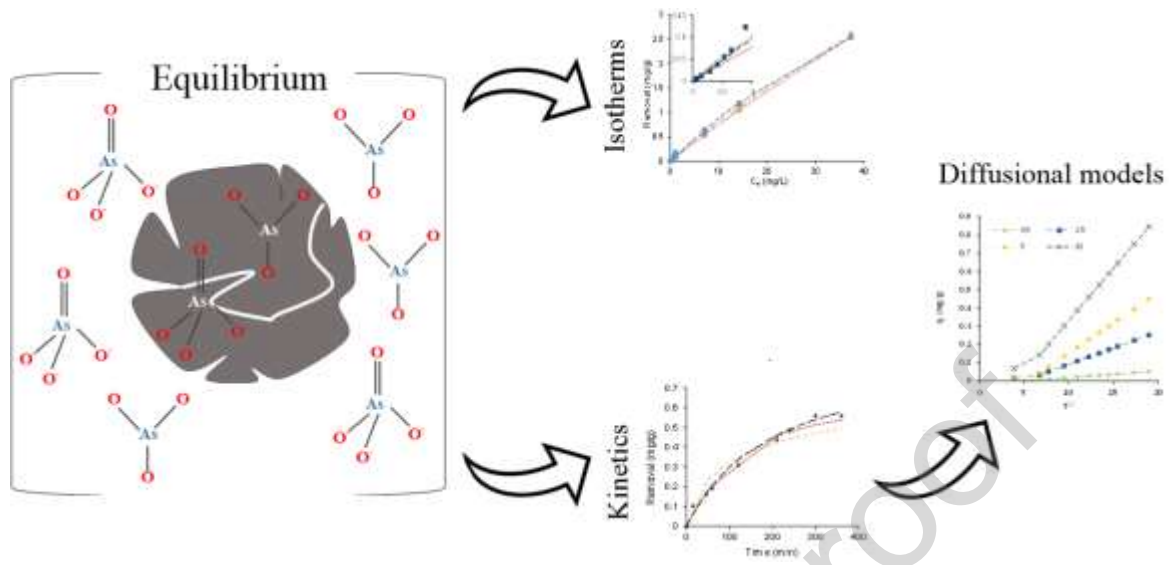
	SSE	HYBRID	MPSD	ARE	SAE
$q_e$	0.054	0.048	0.043	0.048	0.052
$k_2$	0.122	0.122	0.129	0.104	0.100
RSQ	0.851	0.868	0.867	0.878	0.873
SSE	<b>0.001</b>	0.001	0.001	0.001	0.001
HYBRID	0.283	<b>0.244</b>	0.311	0.273	0.219
MPSD	45.640	31.484	<b>29.371</b>	27.943	30.650
ARE	33.187	23.614	22.411	<b>21.183</b>	22.907
SAE	0.057	0.059	0.067	0.062	<b>0.056</b>
SNE	4.283	3.774	4.319	<b>3.928</b>	3.520

## Elovich

	SSE	HYBRID	MPSD	ARE	SAE
$\alpha$	486E-7	491E-7	488E-7	491E-7	469E-7
$\beta$	43.544	48.659	53.939	56.939	44.780
RSQ	0.945	0.945	0.945	0.945	0.945
SSE	<b>0.0001</b>	0.0001	0.000	0.000	0.0001
HYBRID	0.052	<b>0.041</b>	0.048	0.057	0.054
MPSD	19.544	14.035	<b>12.657</b>	13.061	20.181
ARE	11.825	10.373	9.730	<b>9.452</b>	10.63
SAE	0.019	0.019	0.022	0.023	<b>0.017</b>

SNE	4.164	<b>3.693</b>	4.071	4.447	4.121
Ritchie					
	SSE	HYBRID	MPSD	ARE	SAE
$q_e$	0.057	0.062	0.068	0.0752	0.083
$K_R$	0.006	0.004	0.003	0.0026	0.003
RSQ	0.861	0.896	0.916	0.9263	0.918
SSE	<b>0.001</b>	0.001	0.001	0.0006	0.0003
HYBRID	0.263	<b>0.176</b>	0.177	0.1767	0.135
MPSD	27.469	43.772	<b>23.404</b>	22.9378	28.329
ARE	31.745	21.253	17.932	<b>16.9302</b>	20.717
SAE	0.050	0.055	0.049	0.0486	<b>0.040</b>
SNE	4.362	<b>4.203</b>	3.648	3.6120	3.059

## Graphical abstract



**Author Contributions:** S.S. Alkurdi contributed to the conceptualization of the research idea, conducted experiments, data collection, analyses and produced the original draft. Jochen Bundschuh contributed to the conceptualization of the research idea and provided supervision and guidance during the experimental work and writing. Raed A. Al-Juboori provided support and guidance during the experimental work, performed EDS analyses, contributed to data analysis and revised and amended the final draft. Les Bowtell provided support during bone char production and contributed in editing the manuscript. Alla Marchuk provided support for arsenic measurements.

**Declaration of interests**

The authors declare that they have no known competing financial interests or personal relationships that could have appeared to influence the work reported in this paper.

The authors declare the following financial interests/personal relationships which may be considered as potential competing interests:

Journal Pre-proof

**Highlights**

- Removing inorganic arsenic species from water using bone char was investigated.
- Arsenite adsorption onto bone char was systematically studied for the first time.
- Isotherms and kinetics studies were employed to identify the nature of adsorption.
- Intraparticle and pore diffusion models were used to study As-char interaction.
- Initial concentration of both species determines the nature of adsorption.

Journal Pre-proof